CONF-880911--24

TIME CONSTANTS AND TRANSFER FUNCTIONS FOR A HOMOGENEOUS 900 MWt METALLIC FUELED LMR*

CONF-880911--24

DE89 004194

by

K. N. Grimm and D. Meneghetti
EBR-II Division
Argonne National Laboratory
Argonne, Illinois 60439-4820

To be presented
at the
1988 International
Reactor Physics Conference
September 18-21, 1988
Jackson, Wyoming

*Work supported by the U. S. Department of Energy, Civilian Reactor Development, under Contract W-31-109-Eng-38.

Time Constants and Transfer Functions for a Homogeneous 900 MWt Metallic Fueled LMR*

by

K. N. Grimm and D. Meneghetti
EBR-II Division
Argonne National Laboratory
Argonne, Illinois 60439-4820

ABSTRACT

Nodal transfer functions are calculated for a 900 MWt U10Zr-fueled sodium cooled reactor. From the transfer functions the time constants, feedback reactivity transfer function coefficients, and power coefficients can be determined. These quantities are calculated for core fuel, upper and lower axial reflector steel, radial blanket fuel, radial reflector steel, and B_4C radial shield regions. These quantities are also calculated for the control-rod shaft expansion effect. The quantities are compared to the analogous quantities of a 60 MWt metallic-fueled sodium cooled Experimental Breeder Reactor II configuration.

INTRODUCTION

Considerable information can be learned from detailed knowledge of feedback transfer functions of reactors. From specific transfer functions of components, the relative kinetic (or temporal) behavior of specific components can be estimated. For a long time, and with renewed interest since the successful completion of the Inherent Safety Demonstration Test at the Experimental Breeder Reactor II (EBR-II)[1], there has been considerable interest in larger systems having metal fuel. The time constants, feedback reactivity transfer function coefficients, and power coefficients have been calculated, and reported[2], for specific stereotypical subassembly types for the EBR-II reactor. Herein, the analogous quantities are presented for a 900 MWt metallic-fueled sodium cooled reactor. The description of the homo-

*Work supported by the U. S. Department of Energy, Civilian Reactor Development, under Contract W-31-109-Eng-38.

geneous 900 MWt reactor of this study is similar, but not identical, to that of a preliminary reference core design[3]. Some modifications were made to the reactor description to enable use of EBR-II reactivity-feedback coefficient codes; and, some unavailable design parameters needed for the calculation of the feedbacks were assumed[4]. The metallic fuel was assumed to be uranium with 10 weight-percent zirconium (U10Zr).

Power change transfer functions can be obtained from component reactivities given any power change. The analysis, however, is much easier assuming a step change in power. The method used to simulate a step function of power in the EROS[5] kinetics code has been discussed[2]. It was shown that the transfer function, h(t), for a given node (or sum of nodes) can be calculated by

$$h(t) = \frac{1}{a}\frac{\partial \rho(t)}{\partial t} \tag{1}$$

where a is the power step and $\rho(t)$ is the node (or sum of nodes) reactivity. Due to the multiplicity of eigenvalues of the heat equation, the transfer function is composed of many terms:

$$h(t) = \sum_i h_i(o) e^{-t/\tau_i} \tag{2}$$

where $h_i(o)$ is the i-th feedback reactivity transfer function coefficient and τ_i is a time constant. (As in Ref. 2, the values of the $h_i(o)$'s and τ_i's as used herein include the effects of the flowing coolant which may not be part of the node.) Given the transfer function, the power coefficient ($\partial\rho/\partial p$) and the feedback reactivity, $\rho(t)$, are then

$$\frac{\partial \rho}{\partial p} = \frac{1}{p_o} \sum_i h_i(o)\tau_i \tag{3}$$

and

$$\rho(t) = a \sum_i h_i(o)\tau_i \left(1 - e^{-t/\tau_i}\right) \tag{4}$$

where p_o is the initial power. (Also in Ref. 2 analytic estimates were made of these quantities for channel bottom-node positions. The equation for the bottom-node time constant is

$$\tau_i = \frac{r^2}{\beta_i^2 \alpha} \tag{5}$$

where β_i is a number obtainable from film coefficients and thermal resistances outside the radius r and α is the thermal diffusivity.)

The values of time constants (τ_i), transfer function coefficients ($h_i(o)$), and power coefficients ($h_i(o)\tau_i/p_o$) will be given for this 900 MWt metal-fueled LMR system and results compared with corresponding EBR-II values.

EROS MODEL AND CALCULATION

The 900 MWt metallic fueled Liquid Metal Reactor (LMR) configuration analyzed is a 91.4 cm (3 ft) high 7-row core region surrounded by a full-height (335.3 cm; 11 ft) radial depleted U10Zr blanket row (row 8), in turn surrounded by a steel radial reflector (SSR) row (row 9). This is then surrounded by two full-height shielding rows (rows 10 and 11) containing boron carbide. The core subassemblies have upper and lower steel axial reflector regions. Seventeen EROS channels were used to geometrically model this configuration. These are: 7 fueled core channels (one for each core row); a control rod composed of several channels; a radial blanket channel; a radial reflector channel; a radial shield channel; a lower reflector channel; a pin-top (gas plenum) channel; and a channel for the upper reflector. The pin-top region was modeled radially as an argon filled gas space surrounded by cladding. Only one channel, a row 6 lower reflector stereotype, was used to model all the lower reflector axial effects. Two other single channels, separately, were used for the driver pin-top and upper steel reflector regions. Because of axial expansion effects in the control rod shaft (assumed suspended from above), the control rods were modeled with four distinct channels. These channels were equivalent to a steel lower reflector region, steel core region, B_4C region, and steel upper reflector region. Built-in the EROS code are models for the rod-shaft structure above the upper reflector in the outlet plenum region. Geometrical properties and sodium velocities for the channels are shown in Table 1. The sodium bonded metal fuel was assumed to be fresh in all fueled subassemblies.

Table 1. Geometrical Properties and Sodium Velocities of Subassemblies in the 900 MWt Reactor

Subassembly Type	Number of Pins	Gap	Gap Material	Steel OD (cm)	Steel ID (cm)	Fuel OD (cm)	Pin Height (cm)	Na Velocity (cm/s)
Lower Reflector	7	-	-	4.086	-	-	76.2	501.8
Driver	271	open	sodium	0.711	0.620	0.536	91.4	651.0[a]
Pin-top	271	-	-	0.711	0.620	(gas)	101.6	651.0
Upper Reflector	7	-	-	4.086	-	-	66.0	501.7
Control Lower-reflector	37	-	-	2.015	-	-	76.2	209.2
Control Core-section	37	-	-	2.015	-	-	91.4	209.2
Control B_4C	37	-	-	2.015	1.710	1.710 (B_4C)	91.4	209.2
Control Upper-reflector	37	-	-	2.015	-	-	76.2	209.2
Radial Blanket	127	open	sodium	1.163	1.072	0.866	335.3	71.8
Radial Reflector	61	-	-	1.819	-	-	335.3	14.8
Radial Shield	7	-	-	5.178	1.938	1.938 (B_4C)	335.3	9.7

(a) Sodium velocity depends on row. Value shown is for a row 6 subassembly.

In the fueled channels (core or blanket), there were 5 radial mesh intervals: 2 in the U10Zr fuel and 1 each in the bond sodium, steel cladding and sodium coolant. In the pin-top and B_4C channels, there were 4 radial mesh intervals: 2 in the pin-top gas (or B_4C) and 1 each in the steel cladding and sodium coolant. In the steel and sodium channels, there were 3 radial nodes in the steel and 1 node in the sodium coolant. Except for the full-height channels (see Table 1) which had 25 axial nodes, all channels had 10 axial nodes.

The temperature coefficients of reactivity for each channel were obtained using an addition (TEMPCO)[6] to the EBRPOCO[7] code. For each stereotypical channel, reactivity coefficients were calculated for the following effects: (1) coolant density, (2) coolant displacement by structural expansions, (3) steel density, (4) gap sodium temperature and the gap sodium displacement by relative fuel-clad expansions, (5) fuel axial expansion, and (6) fuel Doppler. The coolant density coefficient was attached to the sodium coolant temperature. The coolant displacement and steel density coefficients were attached to the steel temperature. In the fueled channel with an open gap, the gap density and gap sodium displacement coefficient was attached to the gap sodium temperature. Finally, the fuel axial expansion coefficient, along with the fuel Doppler coefficient, were attached to the fuel temperature. In general, temperature coefficients of reactivity were negative except for gap, clad and sodium coolant regions for some non-peripheral core axial nodes of inner core rows.

CALCULATIONAL RESULTS

Methods used to determine the multi-term transfer function have already been discussed[2]. For this analysis a -10% step change in power was used as the initiating event. Multiple (at most 3) terms were calculated by an unpeeling method, from large time constants to small time constants, using a least-squares linear regression fit of the logarithm of the overall transfer function.

CORE FUELED SUBASSEMBLIES

In the 900 MWt LMR case calculations there were 10 equally spaced axial nodes in each of the core fueled channels, the one lower reflector channel, the one pin-top channel and the one upper reflector channel. The multi-term axially dependent time constants, feedback reactivity transfer function coefficients, and power coefficients calculated for the lower reflector steel, core fuel, pin-top steel, and upper reflector steel regions in a row 6 position are shown in Table 2. Shown for each channel are the bottom-node values, top-node values and for the core region, the midplane values. (Also shown in the table are analytic estimates of the time constants, transfer functions coefficients, and power coefficients. These analytic estimates apply only to the lowest node in that particular region.) Shown in Table 3 are row-dependent midplane values for the largest of the three calculated time constants.

Shown in Table 4 for a row 2 position, are the corresponding values for the EBR-II reactor at 60 MWt. The radial (row) dependence of the largest of the three calculated midplane time constants are shown in Table 3. Also shown in Table 3 are the ratios of the 900 MWt LMR case values with the EBR-II case values.

BLANKET/SSR

In the 900 MWt LMR model there is only one row of blanket (row 8) surrounded by one row of radial reflector (row 9). The multi-term axially dependent time constants, feedback reactivity transfer function coefficients and power coefficients calculated for reflector steel and blanket fertile material fuel are shown in Table 5. Values are shown for five equally spaced axial locations. (Also shown in the table are the lower node analytic estimates of these values.)

In EBR-II the core is surrounded by about four rows (rows 7-10) of full-height steel reflector subassemblies and these are surrounded by approximately five full-height full or partial rows of blanket subassemblies. (In the EBR-II model all the radial reflector subassemblies were modeled using one channel based on characteristics from a row 8 subassembly, whereas all the radial

TABLE 2. Axial Variations (Row 6) in the Time Constant, Feedback Reactivity Transfer Function Coefficient, and Power Coefficient for Lower Reflector (L/R) Steel, Core Fuel, Pin-top Steel and Upper Reflector (U/R) Steel Following a 10% Step-drop in Power in the 900 MWt LMR Case (β = 0.0070)

Region	Time Constant, s			Transfer Function Coefficient, $/s			Power Coefficient $/MWt			Total
	$root_1$	$root_2$	$root_3$	$root_1$	$root_2$	$root_3$	$root_1$	$root_2$	$root_3$	
U/R top	17.4	3.42	1.04	-1.4^{-10}	-2.0^{-10}	4.2^{-10}	-2.6^{-12}	-7.6^{-13}	4.9^{-13}	-2.9^{-12}
U/R bottom	17.0	3.08	0.72	-5.1^{-9}	-8.7^{-9}	1.9^{-8}	-9.6^{-11}	-3.0^{-11}	1.5^{-11}	-1.1^{-10}
Plenum top	0.62	0.37	0.16	-3.5^{-6}	5.0^{-6}	-1.5^{-6}	-2.4^{-9}	2.1^{-9}	-2.6^{-10}	-6.1^{-10}
Plenum bottom	0.60	0.28	0.03	-7.5^{-3}	8.1^{-3}	-1.1^{-3}	-5.0^{-6}	2.5^{-6}	-3.7^{-8}	-2.5^{-6}
Core top	0.64	0.42	0.08	-8.9^{-3}	8.0^{-3}	-1.6^{-3}	-6.3^{-6}	3.8^{-6}	-1.3^{-7}	-2.7^{-6}
Core mid	0.56	0.29	0.06	-2.1^{-2}	9.1^{-3}	-5.7^{-3}	-1.3^{-5}	2.9^{-6}	-3.6^{-7}	-1.0^{-5}
Core bottom	0.38	0.24	0.01	-6.1^{-3}	-1.1^{-3}	-1.2^{-3}	-2.6^{-6}	-3.0^{-7}	-1.7^{-8}	-2.9^{-6}
L/R top	17.1	3.22	1.10	-4.6^{-5}	-9.2^{-6}	-7.4^{-6}	-8.7^{-7}	-3.3^{-8}	-9.1^{-9}	-9.1^{-7}
L/R bottom	17.5	1.87	2.35	-4.5^{-8}	-1.8^{-8}	-6.1^{-9}	-8.8^{-10}	-3.7^{-11}	-1.6^{-11}	-9.3^{-10}
U/R analytic	17.1	3.23	1.32	-7.6^{-11}	-1.4^{-11}	-5.7^{-12}	-1.4^{-12}	-5.1^{-14}	-8.3^{-15}	-1.5^{-12}
Core analytic	0.28	0.05	0.02	-7.8^{-3}	-5.9^{-4}	-1.0^{-4}	-2.5^{-6}	-3.0^{-8}	-1.9^{-9}	-2.5^{-6}
L/R analytic	18.1	3.43	1.40	-4.3^{-8}	-8.0^{-9}	-3.2^{-9}	-8.6^{-10}	-3.1^{-11}	-5.0^{-12}	-9.0^{-10}

TABLE 3. Row-dependent Midplane Largest-root Time Constants for the 900 MWt LMR Case Fuel and for the EBR-II Fuel (60 MWt)

Core Row	Midplane Time Constant, s		LMR Value/EBR-II Value
	LMR[a]	EBR-II	
1	0.53	0.15	3.5
2	0.53	0.15	3.5
3	0.55	0.16	3.4
4	0.56	0.19	3.0
5	0.58	0.21	2.8
6	0.56	0.25	2.2
7	0.70	0.25	2.8

(a) 900 MWt U10Zr fueled LMR case.

TABLE 4. Axial Variation (Row 2) in the Time Constant, Feedback Reactivity Transfer Function Coefficient, and Power Coefficient for Lower Reflector (L/R) Steel, Core Fuel, Plenum Steel and Upper Reflector (U/R) Steel Following a 10% Step Drop in Power in EBR-II RUN 93A (60 MWt) (β = 0.0068)

Region	Time Constant, s			Transfer Function Coefficient, $/s			Power Coefficient $/MWt			Total
	$root_1$	$root_2$	$root_3$	$root_1$	$root_2$	$root_3$	$root_1$	$root_2$	$root_3$	
U/R top	21.5	3.45	0.83	-2.4^{-7}	-3.9^{-7}	-1.3^{-6}	-8.7^{-8}	-2.2^{-8}	-1.8^{-8}	-1.3^{-7}
U/R bottom	21.3	3.41	0.80	-2.1^{-5}	-2.9^{-5}	-1.1^{-4}	-7.3^{-6}	-1.7^{-6}	-1.4^{-6}	-1.0^{-5}
Plenum top	0.16	0.08	0.04	-6.2^{-3}	1.2^{-2}	-6.0^{-3}	-1.7^{-5}	1.5^{-5}	-3.7^{-6}	-5.7^{-6}
Plenum bottom	0.16	0.06	0.17	-4.7^{-2}	5.3^{-2}	3.2^{-3}	-1.3^{-4}	5.6^{-5}	9.0^{-6}	-6.1^{-5}
Core top	0.18	0.10	0.01	-1.4^{-3}	1.2^{-3}	-5.6^{-4}	-4.2^{-6}	1.9^{-6}	-2.7^{-7}	-2.5^{-6}
Core mid	0.15	0.06	0.03	-1.7^{-3}	9.4^{-4}	-7.0^{-4}	-4.3^{-6}	1.0^{-6}	-2.9^{-7}	-3.6^{-6}
Core bottom	0.10	0.04	-	-8.5^{-4}	-8.6^{-6}	-	-1.5^{-6}	-5.1^{-9}	-1.1^{-7}	-1.6^{-6}
L/R top	19.6	2.52	0.27	-7.3^{-4}	-2.2^{-4}	-2.2^{-4}	-2.4^{-4}	-9.4^{-6}	-1.0^{-6}	-2.5^{-4}
L/R bottom	20.4	1.10	1.24	-1.9^{-7}	-1.6^{-7}	-3.9^{-7}	-6.6^{-8}	-2.8^{-9}	-8.0^{-9}	-7.6^{-8}
U/R analytic	22.2	4.21	1.71	-2.3^{-6}	-4.4^{-7}	-1.8^{-7}	-8.6^{-7}	-3.1^{-8}	-5.1^{-9}	-9.0^{-7}
Core analytic	0.09	0.01	0.01	-9.3^{-4}	-7.1^{-5}	-1.2^{-5}	-1.3^{-6}	-1.7^{-8}	-1.1^{-9}	-1.3^{-6}
L/R analytic	19.6	3.71	1.51	-2.0^{-7}	-3.8^{-8}	-1.5^{-8}	-6.6^{-8}	-2.4^{-9}	-3.9^{-10}	-6.8^{-8}

TABLE 5. Axial Variations in the Time Constant, Feedback Reactivity Transfer Functica Coefficient, and Power Coefficient for Radial Reflector (Row 9) Steel and Blanket (Row 8) Fuel Following a 10% Step Drop in Power in the 900 MWt LMR Case

Region	Time Constant, s			Transfer Function Coefficient, $/s			Power Coefficient, $/MWt			Total
	$root_1$	$root_2$	$root_3$	$root_1$	$root_2$	$root_3$	$root_1$	$root_2$	$root_3$	
SSR top	148.	84.2	39.3	-1.0^{-11}	4.2^{-11}	-2.1^{-10}	-1.7^{-12}	3.9^{-12}	-9.2^{-12}	-7.0^{-12}
SSR	107.	61.4	16.5	-5.4^{-9}	1.9^{-8}	-3.3^{-6}	-6.4^{-10}	1.3^{-9}	-6.0^{-8}	-5.9^{-8}
SSR mid	111.	61.4	20.1	-4.5^{-7}	4.3^{-7}	-4.3^{-8}	-5.6^{-8}	2.9^{-8}	-9.6^{-10}	-2.7^{-8}
SSR	64.9	24.5	0.5	-3.0^{-7}	8.5^{-8}	-2.6^{-6}	-2.2^{-8}	2.3^{-9}	-1.5^{-9}	-2.1^{-8}
SSR bottom	13.3	-	-	-2.3^{-10}	-	-	-3.4^{-12}	-	-	-3.4^{-12}
Blkt top	18.2	8.7	5.1	-6.7^{-9}	6.3^{-8}	-2.7^{-7}	-1.4^{-10}	6.0^{-10}	-1.5^{-9}	-1.1^{-9}
Blkt	12.3	6.4	4.8	-1.9^{-6}	1.0^{-5}	-1.0^{-5}	-2.6^{-8}	7.2^{-8}	-5.6^{-8}	-9.9^{-9}
Blkt mid	9.8	3.2	2.7	-5.1^{-5}	6.3^{-5}	-2.6^{-5}	-5.5^{-7}	2.2^{-7}	-7.7^{-8}	-4.1^{-7}
Blkt	5.4	3.0	0.2	-4.9^{-5}	-2.4^{-5}	-3.3^{-5}	-3.0^{-7}	-7.9^{-8}	-6.7^{-9}	-3.8^{-7}
Blkt bottom	0.8	0.6	0.2	-3.9^{-7}	-3.8^{-7}	-1.2^{-7}	-3.6^{-10}	2.4^{-10}	-2.4^{-11}	-1.5^{-10}
SSR analytic	3.5	0.7	0.3	-4.9^{-11}	-9.3^{-12}	-3.7^{-12}	-1.9^{-13}	-6.8^{-15}	-1.1^{-15}	-2.0^{-13}
Blkt analytic	0.6	0.1	0.04	-7.6^{-8}	-7.4^{-9}	-1.5^{-9}	-5.2^{-11}	-8.8^{-13}	-6.7^{-14}	-5.3^{-11}

blanket subassemblies were modeled using one channel based on a row 10 blanket subassembly.) The multi-term axially dependent time constants, feedback reactivity transfer function coefficients, and power coefficients are shown in Table 6. (Also shown are the analytic bottom node estimates of these values.) Additional calculations were made to compare the row dependence of the time constants in the EBR-II radial reflector. These values vary radially because each row has a different flow rate. Shown in Fig. 1 is the axial dependence of the largest root of the row-dependent time constant in the EBR-II radial reflector steel.

CONTROL-ROD SHAFT EXPANSION

The poison control rod assemblies have 37 pins. Each pin has a lower 167.6 cm (5.5 ft) section of steel followed by a 91.4 cm (3 cm) section containing the encapsulated B_4C, then followed by a 60.4 cm (2 ft) section of steel.

The shaft expansion effect is modeled by four axial lengths. The first term (L_1) is associated with axial expansion of the control-rod hex-shaped assembly from the bottom of the poison section to the tops of the surrounding ducts of the core subassemblies. The other lengths (L_2-L_4) model axial effects above this level to approximately the top of the vessel (not the top of the surrounding pool tank). The total shaft expansion is calculated explicitly for the L_1 region and implicitly for the L_2-L_4 sections. Once the expansion overall length is calculated, the reactivity is then the incremental length multiplied by an input worth per unit length value. This worth per unit length was calculated to be -0.16\$/cm (-4.79\$/ft). The calculated time constants, feedback reactivity transfer function coefficients and power coefficients for L_1-L_4 sections are shown in Table 7.

An EBR-II standard control-rod assembly has 61 fuel pins. Each pin has a lower reflector region, a Mk-IA fueled section, a pin-top section, and a upper reflector region. Since the diameter of the Mk-IA fuel of the control rods of Run 93A is somewhat larger in diameter than the Mk-II fuel in the driver subassemblies, the time constants for the Mk-IA fuel will be somewhat larger than the Mk-II driver fuel time constants given in Table 4. (For example, the analytic (bottom node) estimate for the time constant of fresh Mk-II fuel in row 5 is 0.095 s, whereas the corresponding time constant for fresh Mk-IA fuel

TABLE 6. Axial Variations in the Time Constant, Feedback Reactivity Transfer Function Coefficient, and Power Coefficient for Radial Reflector (Row 8) Steel and Blanket (Row 10) Fuel Following a 10% Step Drop in Power in EBR-II Run 93A (60 MWt)

Region	Time Constant, s			Transfer Function Coefficient, $/s			Power Coefficient $/MWt			Total
	$root_1$	$root_2$	$root_3$	$root_1$	$root_2$	$root_3$	$root_1$	$root_2$	$root_3$	
SSR top	95.8	24.5	11.1	-7.7^{-7}	1.1^{-6}	-3.4^{-7}	-1.2^{-6}	4.4^{-7}	-6.3^{-8}	-8.5^{-7}
SSR	67.4	25.1	4.8	-1.1^{-5}	8.8^{-6}	4.8^{-7}	-1.3^{-5}	3.7^{-6}	3.8^{-8}	-9.1^{-6}
SSR mid	47.7	17.6	3.8	-8.4^{-5}	5.1^{-6}	-2.1^{-6}	-6.7^{-5}	1.5^{-6}	-1.2^{-7}	-6.5^{-5}
SSR	42.0	4.6	0.2	-3.7^{-6}	-4.4^{-7}	-8.8^{-6}	-2.6^{-6}	-3.4^{-8}	-3.2^{-8}	-2.7^{-6}
SSR bottom	32.8	1.7	0.5	-2.5^{-8}	-4.8^{-8}	-3.5^{-7}	-1.4^{-8}	-1.3^{-9}	-2.6^{-9}	-1.7^{-8}
Blkt top	65.0	19.0	6.1	-9.8^{-7}	1.5^{-6}	-8.1^{-7}	-1.1^{-6}	4.7^{-7}	-8.3^{-8}	-6.8^{-7}
Blkt	31.2	8.1	4.9	-5.7^{-6}	1.8^{-5}	-1.8^{-5}	-2.9^{-6}	2.4^{-6}	-1.4^{-6}	-2.0^{-6}
Blkt mid	9.9	7.8	4.1	-5.4^{-4}	7.4^{-4}	-3.4^{-4}	-8.9^{-5}	9.6^{-5}	-2.3^{-5}	-1.5^{-5}
Blkt	6.8	4.9	4.4	-1.3^{-5}	1.3^{-5}	-5.3^{-6}	-1.5^{-6}	1.1^{-6}	-3.8^{-7}	-7.9^{-7}
Blkt bottom	2.0	0.1	0.1	-7.4^{-8}	-1.8^{-7}	1.5^{-7}	-2.5^{-9}	-2.6^{-10}	1.4^{-10}	-2.6^{-9}
SSR analytic	31.3	6.0	2.4	-2.4^{-8}	-4.5^{-9}	-1.8^{-9}	-1.2^{-8}	-4.5^{-10}	-7.4^{-11}	-1.3^{-8}
Blkt analytic	0.7	0.1	0.1	-5.8^{-8}	-8.4^{-9}	-2.4^{-9}	-7.0^{-10}	-1.9^{-11}	-2.1^{-12}	-7.2^{-10}

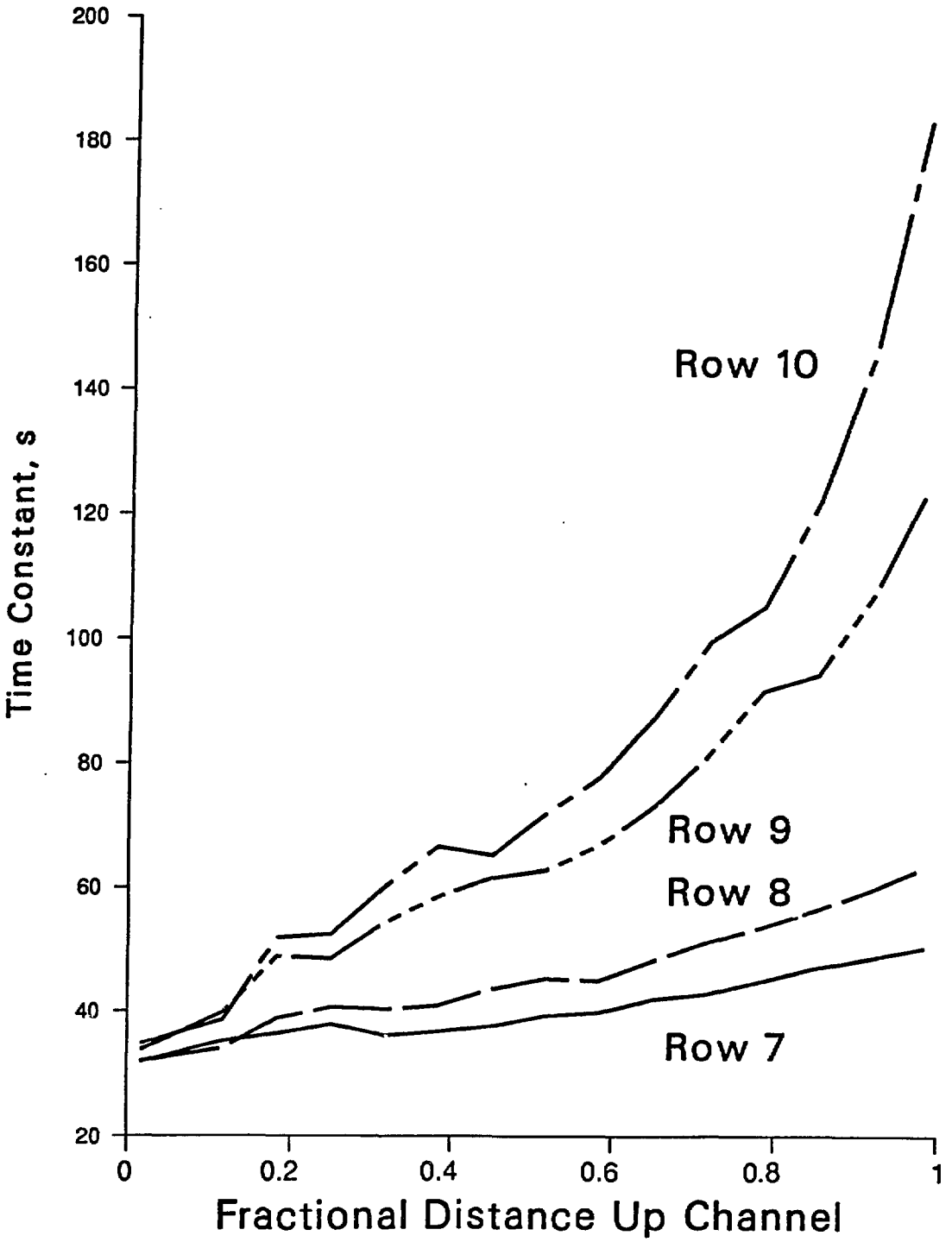

Figure 1. Axial Dependence of Largest Root Time Constant for Steel in EBR-II Radial Reflector Rows 7 through 10

TABLE 7. Control-Rod-Shaft Time Constants, Feedback Reactivity Transfer Function Coefficient, and Power Coefficient following a 10% Step Drop in Power in the 900 MWt LMR Case and a 60 MWt EBR-II

Region	Time Constant, s			Transfer Function Coefficient, $/s			Power Coefficient $/MWt			Total
	$root_1$	$root_2$	$root_3$	$root_1$	$root_2$	$root_3$	$root_1$	$root_2$	$root_3$	
LMR L_1	8.3	5.1	2.7	-4.3^{-3}	3.4^{-3}	-5.5^{-4}	-4.0^{-5}	1.9^{-5}	-1.3^{-6}	-2.2^{-5}
LMR L_2	8.5	6.5	2.7	-3.6^{-3}	4.3^{-3}	-7.5^{-4}	-3.4^{-5}	3.1^{-5}	-2.3^{-6}	-5.0^{-6}
LMR L_3	21.2	10.2	5.3	-7.1^{-4}	1.2^{-3}	-5.1^{-4}	-1.7^{-5}	1.4^{-5}	-3.0^{-6}	-6.0^{-6}
LMR L_4	9.3	7.5	4.7	-8.8^{-3}	1.2^{-2}	-3.3^{-3}	-9.1^{-5}	1.0^{-4}	-1.7^{-5}	-6.9^{-6}
EBR L_1	16.9	1.2	0.2	-1.7^{-5}	-4.8^{-3}	-5.0^{-1}	-4.8^{-6}	-9.1^{-5}	-1.9^{-3}	-2.0^{-3}
EBR L_2	2.1	0.2	0.2	-9.0^{-3}	5.4^{-2}	-5.3^{-2}	-3.1^{-4}	2.1^{-4}	-1.3^{-4}	-2.4^{-4}
EBR L_3	21.1	2.0	1.5	-9.9^{-4}	1.2^{-3}	2.1^{-4}	-3.5^{-4}	3.9^{-5}	5.5^{-6}	-3.0^{-4}
EBR L_4	8.2	1.9	0.2	-3.2^{-3}	4.2^{-3}	-2.5^{-3}	-4.3^{-4}	1.3^{-4}	-9.2^{-6}	-3.1^{-4}

is 0.102 s.) The time constants for the steel of the axial reflector regions in the control rods is approximately 2 seconds whereas the steel in the axial reflector of the drivers have time constants that are approximately 20 seconds. This difference is primarily due to the bulkier reflector steel sections in the driver subassemblies.

The calculated time constants, transfer function coefficients, and power coefficients for the L_1-L_4 terms in the EBR-II reactor are shown in Table 7. For Run 93A, given the specific control-rod positions, the worth-per-unit-length was calculated to be -0.18 \$/cm (-5.52 \$/ft).

SHIELD

In the 900 MWt LMR model the radial reflector row was followed by two rows (rows 10-11) of B_4C-containing shielding subassemblies. The calculated midplane value for the B_4C section was approximately 100 s. (The largest root analytic (bottom-node) time constant for the B_4C region was 19 s.) The EBR-II reactor does not have corresponding poison shielding subassemblies beyond the radial blanket rows.

DISCUSSION AND CONCLUSIONS

The largest-root time constants for core fuel are approximately three times greater than corresponding values for the EBR-II Mk-II fuel. This difference is primarily due to the larger diameter of the fuel. A second contributor to this difference is the relatively larger value of fuel heat capacity. These make the thermal diffusivity smaller, and hence, the time constant relatively larger (see eq. 5). (In the 900 MWt case calculations the value of largest time constant in the fuel at the core bottom is 36% larger than the analytically calculated value; and, in the EBR-II calculations the calculated value is 11% larger than the analytically calculated value. These smaller analytic values result because of the neglect of the sodium coolant heating in the lower reflectors in the analytical model.)

The row-dependent midplane first-root (largest-root) time constants for EBR-II vary much more rapidly than the corresponding 900 MWt case values.

This is because the row power-to-flow ratio (mainly the flow) varies much more rapidly in EBR-II. (In the 900 MWt case the power-to-flow ratio was nearly constant for all rows.)

Shown in Fig. 2 for the 900 MWt case and the EBR-II case are the upper and lower bounds for the ratio of the largest of the three calculated roots of the time constant relative to the core bottom value plotted versus fractional height up the channel. It is seen that the bounds are nearly identical even though the 900 MWt case fuel section height is much larger than the EBR-II fuel section height.

The time constants for the upper and lower reflector steel regions are nearly axially independent. This is not true for the transfer function coefficients in these regions. The transfer function coefficients vary because they reflect the axial worth of the materials. (The analytic estimate for the transfer function coefficient in the upper axial reflector for either the 900 MWt case or the EBR-II case is considerably different than the calculated value because the basic assumptions used to calculate the analytic coefficients do not apply in these regions.)

The bottom node largest-root time constant in both the 900 MWt case SSR steel reflector and the blanket regions are smaller than the corresponding EBR-II values because of the relative diameters of the pins. The relatively large value of time constant for the EBR-II radial reflector steel is due to the relatively large dimension of the single radial reflector rod. In the blanket the thermal diffusivity of the depleted U10Zr fuel would tend to make the blanket time constant larger, but the smaller fuel pin diameter overcomes this to make the time constant smaller. In both the blanket and radial steel reflector, time constants increase significantly from the subassembly bottom to the subassembly top. This is the result of the small sodium coolant velocities in these subassemblies. In the 900 MWt case SSR steel region the largest root time constant increased axially by a factor of about 40 whereas in the EBR SSR steel region this factor is about 3. This larger time constant increase in the 900 MWt case steel region is due to the relatively slower sodium coolant velocity in the radial reflector channel (30 cm/s over 35 cm in height for EBR-II versus 15 cm/s over 335 cm in height for 900 MWt case). In the blanket fuel, the largest-root time constant increased axially by a factor of 30 in the 900 MWt case whereas in the EBR-II blanket fuel this factor is

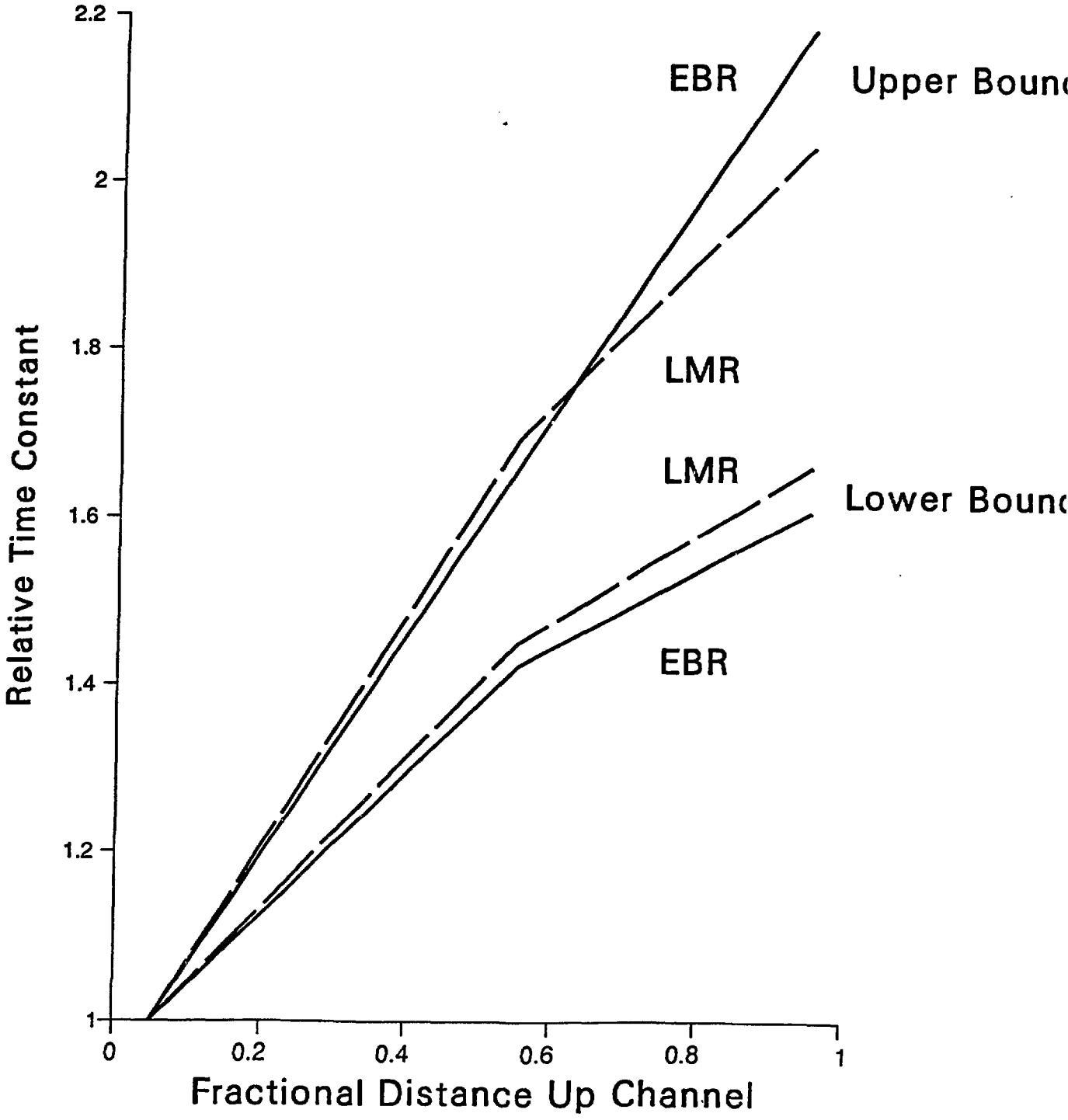

Figure 2. Upper and Lower Bounds for the Fractional Increase in Largest Root Time Constant (relative to bottom-node) value) for Core Rows in the 900 MWt LMR Case and 60 MWt EBR-II

about 90. This is again due to the relatively slower sodium coolant velocity in the EBR-II blanket channel (42 cm/s over 35 cm in height for EBR-II versus 72 cm/s over 335 cm in height for 900 MWt case).

In all the analysis presented here, a maximum of three terms was used to define the transfer function. For the locations with large relative time constants (i.e. higher regions in the radial reflector and radial blanket) more than three terms may be needed to sufficiently define the overall transfer function. For these positions, three terms may correctly define the transfer function at long times (because of the nature of the unpeeling method used to calculate time constants) but additional terms would be needed to define the transfer function at shorter times closer to the initiating power change.

For both reactor cases, a large fraction of the control-rod shaft expansion reactivity is due to the expansion of components above the top of the subassembly hex cans. In the 900 MWt case model the above hex-can components (L_2-L_4) account for approximately 40% of the total shaft expansion reactivity effect whereas in the EBR-II model the L_2-L_4 components accounted for approximately 60% of the control rod shaft expansion reactivity. This difference is due to the relatively longer length of the L_1 component in the 900 MWt case model. Because detailed design parameters are not known for the LMR shaft hardware, the portions of the LMR control rod shaft above the subassembly hex cans (L_1-L_4) were taken to be identical to the corresponding EBR-II values. Since the physical size of the LMR control rod assembly is much larger than that in EBR-II (outer hex-can flat-to-flat dimension: LMR 13.60 cm, EBR-II 4.85 cm), the shaft hardware could be more substantial. In this case then the time constants shown in Table 7 for the LMR L_2-L_4 components would be larger (see eq. 5).

The calculational results presented herein for the 900 MWt case used a -10% step change in power. EBR-II values were calculated using both a -10% step and a +10% step change in power[2]. The differences in time constant, transfer function coefficient, and power coefficient were negligible between the +10% and -10% case.

Presented here have been time constants calculated only for regions where energy was assumed deposited. (In fueled regions, all energy was assumed deposited in the fuel.) It was seen in the EBR-II analysis results that the

time constants in non-energy-deposition regions (i.e., cladding in fueled regions and coolant regions) varied slightly but not significantly from the time constants where energy was assumed to be deposited[8]. This is primarily due to the relatively thin cladding regions and the relatively large values of coolant conductivity.

The time constants and feedback reactivity transfer function coefficients presented here for the 900 MWt case U10Zr core fuel assume fresh fuel. If the fuel is assumed expanded to the clad, then the time constants of the fuel (assuming no bond sodium leakage into the fuel porosity) will decrease by ~ 10%. (Since the conductivity of sodium is larger than the conductivity of U10Zr fuel, there may be an increase in the time constant if there is sufficient sodium leakage into the porosity of the fuel.) If in addition to expanding to the clad, the fuel is assumed adhering to the clad, then that part of the fuel feedback reactivity transfer function coefficient due to fuel axial expansion has to be reduced by ~ 40% because fuel axial expansion is then determined by axial expansion of the cladding.

(The steel linear thermal expansion coefficients that were used in calculating the steel temperature coefficients are given in Ref. 4. Feedback reactivity transfer function coefficients for steel regions assuming different linear expansion coefficients can be obtained by multiplying by the ratio of the desired expansion coefficient to that expansion coefficient assumed herein.)

REFERENCES

(1) H. P. Planchon, J. I. Sackett, G. H. Golden and R. H. Sevy, "Implications of the EBR-II Inherent Safety Demonstration Test," Nucl. Engrg. Des., 101, 75 (1987).

(2) K. N. Grimm and D. Meneghetti, "Time Constants and Feedback Transfer Functions of EBR-II Subassembly Types," Ann. Nucl. Energy, Vol. 14, No. 9, pp. 481-487, 1987.

(3) Y. Orechwa and H. Khalil, "Physics Implications of Oxide and Metal Fuels on the Design of Small LMFBR Cores," Topl. Mtg. on Reactor Physics and Shielding, I, ISBN: 089448-113-4, 323 (1984).

(4) D. Meneghetti and D. A. Kucera, "Reactivity Feedback Components of a Homogeneous U10Zr-Fueled 900 MWt LMR," Proc. Topl. Mtg. Safety of Next Generation Power Reactors, to be published (1988).

(5) E. M. Dean and H. A. Larson, "EROS: An Experimental Breeder Reactor II Operating Safety Code," Nucl. Technol., 57, 1, 7 (Apr. 1982).

(6) D. Meneghetti and D. A. Kucera, "Calculation of Temperature Coefficients of Reactivity for EBR-II Kinetics Analysis, Ann. Nucl. Energy, Vol. 14, No. 12, pp. 663-671, 1987.

(7) D. Meneghetti and D. A. Kucera, "EBRPOCO - A Program to Calculate Detailed Contributions of Power Reactivity Components of EBR-II," Proc. Intl. Topl. Mtg. Advances in Mathematical Methods for the Solution of Nuclear Engineering Problems, 2, 225, (1981).

(8) K. N. Grimm and D. Meneghetti, "EBR-II Time Constant Calculation Using the EROS Kinetics Code," Trans. Am. Nucl. Soc., 52, p. 656 (1986).